Strength and Plastic Rotation Capacity of I-Shaped Beams with Grid-Purlin System Subjected to Cyclic Loading

Ryota Matsui[1]; Koichi Koizumi[2]; Pao-Chun Lin[3]; Masanobu Iwanaga[4]; An-Chien Wu[5]; Toru Takeuchi, A.M.ASCE[6]; and Keh-Chuyan Tsai, A.M.ASCE[7]

Abstract: This paper introduces a grid-purlin system, which was composed of secondary rectangular-hollow-section grids welded onto the top flange of I-shaped beams of moment frames. The welded grid-purlin itself may play a role of a lateral bracing member for the welded beam. However, the ultimate strength, plastic rotation capacity, or other structural characteristics of this grid-purlin system remain poorly understood. This paper presents two full-scale cyclic loading tests on specimens with I-shaped beams 700 mm deep, 240 mm wide, and 13 m long. The diagonal length of grids in the square grid-purlin of the specimen was 1.3 m on-center, and two different depths of the sections were selected for the purlin sections. Both specimens successfully achieved fully plastic moments at a plastic rotation exceeding 0.04 rad. This shows that the grid-purlin system provides reliable lateral bracing. Continuum finite-element (CFE) analysis was performed to simulate the hysteretic experimental response of the grid-purlin system. This CFE model was used to examine the plastic rotation capacity for a variety of combinations of I-shaped beams and grid-purlins. **DOI: 10.1061/(ASCE)ST.1943-541X.0003017.**

Author keywords: Beam; Purlin; Stability bracing of beams; Plastic rotation capacity; Cyclic loading test.

Introduction

Instability can govern the inelastic deformation capacity of steel beams in moment frames. The ANSI/AISC 360-16 specification (AISC 2016b) stipulates requirements for the maximum unbraced lengths for which portions of beams can be used to form a plastic mechanism. As reported in Yura et al. (1978), the maximum unbraced length for moment redistribution in that ANSI/AISC 360-16 (AISC 2016b) was based on experimental data (Bansal 1971). The specification provides the maximum permitted unbraced length for steel members of several forms of section subjected to strong-axis bending. In Appendix 6 of ANSI/AISC 360-16 (AISC 2016b), provisions on member stability bracing also address the minimum strength and stiffness required at the braced point of a beam. Stiffness and strength requirements for lateral bracing are based primarily on recommendations (Yura 2001). Ductile steel beams used in seismic regions need to meet additional requirements for the stability bracing of beams. The seismic provisions ANSI/AISC 360-16 (AISC 2016b) specifies the maximum unbraced lengths for beams in moment frames to withstand plastic rotations without a significant loss of strength. Nakashima et al. (2002) indicated that the requirements for stability bracing of beams in ANSI/AISC 341-16 (AISC 2016a) were reasonably conservative to ensure sufficient plastic rotation capacity. Okazaki et al. (2006) discussed current stability requirements in ANSI/AISC 341-16 (AISC 2016a) from the viewpoint of sustaining plastic moment strength of steel beams at a story drift of 0.04 rad based on an analytical study (Liu et al. 2003). Kimura et al. (2013) performed an eigenvalue analysis based on the energy method to evaluate the continuous bracing of a metal deck for rotation capacity. This research demonstrated that providing an adequate lateral support member overcomes these instability issues and significantly enhances the deformational capacity of beams.

Closely spaced bracing using secondary elements has the potential to improve rotation capacity of bare steel beams in moment frames. Fig. 1 shows a gymnasium roof using an I-shaped beam framing system braced by rectangular hollow section purlins welded to the top flange of the beams. The composition of these purlins is hereafter referred to as the grid-purlin, and the structural system using the grid-purlins as a grid-purlin system. The grid-purlin system is commonly utilized as a nonstructural system to support the roof finishing or the cladding. Thus, this system could be cost competitive because it can completely eliminate the fabrication and erection costs of the secondary beams, roof braces, and the connections between conventional purlins. However, the effects of bracing the beams using grid-purlins have not been determined. This paper describes quasi-static cyclic loading tests of full-scale I-shaped beams with a grid-purlin. The objective of the test program was to verify the strength and plastic rotation capacity of I-shaped beams with a grid-purlin. A continuum finite-element model (CFEM) was

[1]Associate Professor, Graduate School of Engineering, Hokkaido Univ., A5-04, Kita 13-Nishi 8 Kita-ku Sapporo, Hokkaido 060-8628, Japan (corresponding author). ORCID: https://orcid.org/0000-0002-3841-2540. Email: ryota.matsui@eng.hokudai.ac.jp

[2]Formerly, Graduate Student, Dept. of Architecture and Building Engineering, Tokyo Institute of Technology, M1-29, 2-12-1 O-okayama, Meguro-ku, Tokyo 152-8552, Japan.

[3]Assistant Professor, Dept. of Civil Engineering, National Cheng Kung Univ., No. 1, University Rd., Tainan 701, Taiwan. ORCID: https://orcid.org/0000-0001-5389-5192

[4]Principal, Kyushu Daiichi Industry Co., Ltd., 672 Arisa Kagamimachi, Yashiro-shi, Kumamoto 869-4213, Japan.

[5]Associate Researcher, National Center for Research on Earthquake Engineering, No. 200, Section 3, Xinhai Rd., Taipei 106, Taiwan.

[6]Professor, Dept. of Architecture and Building Engineering, Tokyo Institute of Technology, M1-29, 2-12-1 O-okayama, Meguro-ku, Tokyo 152-8552, Japan.

[7]Professor, Dept. of Civil Engineering, National Taiwan Univ., No. 1 Section 4, Roosevelt Rd., Da'an District, Taipei 10617, Taiwan.

Note. This manuscript was submitted on April 2, 2020; approved on January 20, 2021; published online on May 8, 2021. Discussion period open until October 8, 2021; separate discussions must be submitted for individual papers. This paper is part of the ***Journal of Structural Engineering***, © ASCE, ISSN 0733-9445.

Fig. 1. Construction example of grid-purlin roof. [Reprinted with permission from Takeuchi et al. (2019).]

calibrated to reproduce the postbuckling behavior of the I-shaped beam with the grid-purlin. This CFEM was used to evaluate the performance of a variety of I-shaped beam sections with a grid-purlin.

Full-Scale Test of Wide Flange Beams with Grid-Purlin

This section presents the experimental performance of beams with grid-purlin subjected to cyclic loading. The key experimental responses, including flexural strength, plastic rotation capacity, and lateral-torsional buckling-induced deformation, are discussed.

Scheme of Test Program

Fig. 2(a) illustrates the reference area corresponding to the test specimens of an I-shaped beam with the grid-purlin in a gymnasium. The distance from the ridge to the eave was assumed to be 13 m. The specimens measured 6.5 m wide and 13 m long [shaded area in Fig. 2(a)]. A built-up I-shaped beam, WF-700 × 240 × 12 × 22, was used for the beam section of each specimen. RHS-150 × 75 × 3.2 and RHS-75 × 75 × 2.3 were used for the purlin sections of Specimens P150 and P75, respectively. The tests were conducted in the Architecture and Building Research Institute (ABRI) in Taipei in 2018. As shown in Figs. 3 and 4, the specimen was anchored to the strong floor and bending moment was applied as illustrated in Fig. 2(b). The actuator at Point C in Fig. 3 applied vertical loads to the end of the specimens. The boundary conditions at the edge of the purlin and the pin-roller support were constructed

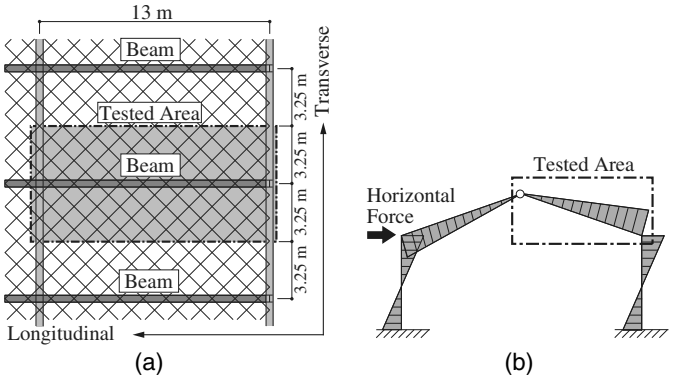

Fig. 2. Extracting specimen from a gymnasium: (a) reference area; and (b) bending moment diagram.

using the connection details shown in Fig. 5. The grid-purlin was connected to the top flange of the I-shaped beam by welding steel plates, as shown in Fig. 6.

Tables 1–3 presents the dimensions and material properties along with the maximum lateral bracing spacing, L_b, for moderately and highly ductile beams, where the σ_y is the yield strength, σ_u is the tensile strength, and M_p is the fully plastic moment. According to ANSI/AISC 341-16 (AISC 2016a), the bracing of ductile beam members shall have a maximum spacing of $L_b = 0.095 r_y E/(R_y F_y)$ for highly ductile members or $0.19 r_y E/(R_y F_y)$ for moderately ductile members, where L_b is the spacing between points that are either braced against lateral displacement of the compression flange or braced against twist of the cross section, r_y is the radius of gyration about the minor axis, E is the elastic modulus, R_y is the ratio of the expected yield stress to the nominal yield stress, and F_y is the specified yield strength. Calculations of L_b used the average yield strength between the flange and web instead of $R_y F_y$ and the average elastic modulus between the flange and web. The fully plastic moment of the I-shaped section, M_p, was calculated from Eq. (1)

$$M_p = Bt_f(H - t_f)\sigma_{y,f} + \frac{1}{4}t_w(H - 2t_f)^2\sigma_{y,w} \tag{1}$$

where H, B, t_w, and t_f are the beam width and depth and web and flange thickness, respectively. The $\sigma_{y,f}$ and $\sigma_{y,w}$ are the yield strength of the flanges and the web, respectively (Table 2). Note that the I-shaped beam without grid-purlins did not satisfy the stability bracing requirements for either highly or moderately ductile members. This clearly indicates that the ductility of the I-shaped beam without grid-purlins was not expected. The Japanese Industrial Standard Steel Grade SS400 was used for the I-shaped flange beams, and STKR400 was used for all the purlins. The specimens were subjected to single curvature bending consistent with a loading protocol (Fig. 7). The loading was controlled by the rotations at Point B (Fig. 3). The amplitude was normalized by the fully plastic yield rotation of the I-shaped beam, θ_p, which was computed from the ratio of the fully plastic moment of the I-shaped beam, M_p, to the flexural stiffness, K. The amplitude was increased from $0.25\theta_p$ to $0.5\theta_p$, $0.75\theta_p$, θ_p, $3\theta_p$, and $5\theta_p$.

Test Results

Fig. 8 illustrates hysteretic response curves of Specimens P75 and P150, which plot the flexural moment, M, against rotation, θ, at Point B shown in Fig. 3. The flexural moment was equal to the vertical force at the actuator multiplied by the horizontal distance between the Points B and C shown in Fig. 3. In this study, positive loading and negative loading represent compression and tension states of the bottom flange of the I-shaped beam, respectively. The flexural stiffness of both Specimens P75 and P150 was computed to be $K = 65{,}000$ kN · m/rad using the first six cycles in the elastic range. The fully plastic yield rotation of the beam was $\theta_p = 0.0221$ rad. The photographs in Fig. 9 show the deformations and damage conditions of the specimens. After the beam reached the fully plastic bending moment, M_p, lateral buckling occurred [Fig. 9(a)] in Specimen P150 during the $+3\theta_p$ (0.0664 rad) cycle. Local buckling of the top flange was observed at approximately $+5\theta_p$ [0.111 rad; see Fig. 9(b)].

Fig. 8(a) shows that Specimen P150 developed a maximum strength larger than the fully plastic moment, M_p, without any secondary beams for lateral bracing in the positive part of the ninth cycle [Point (a)]. The bending strength remained larger than the fully plastic moment, M_p, until the rotation, θ, reached 0.0637 rad

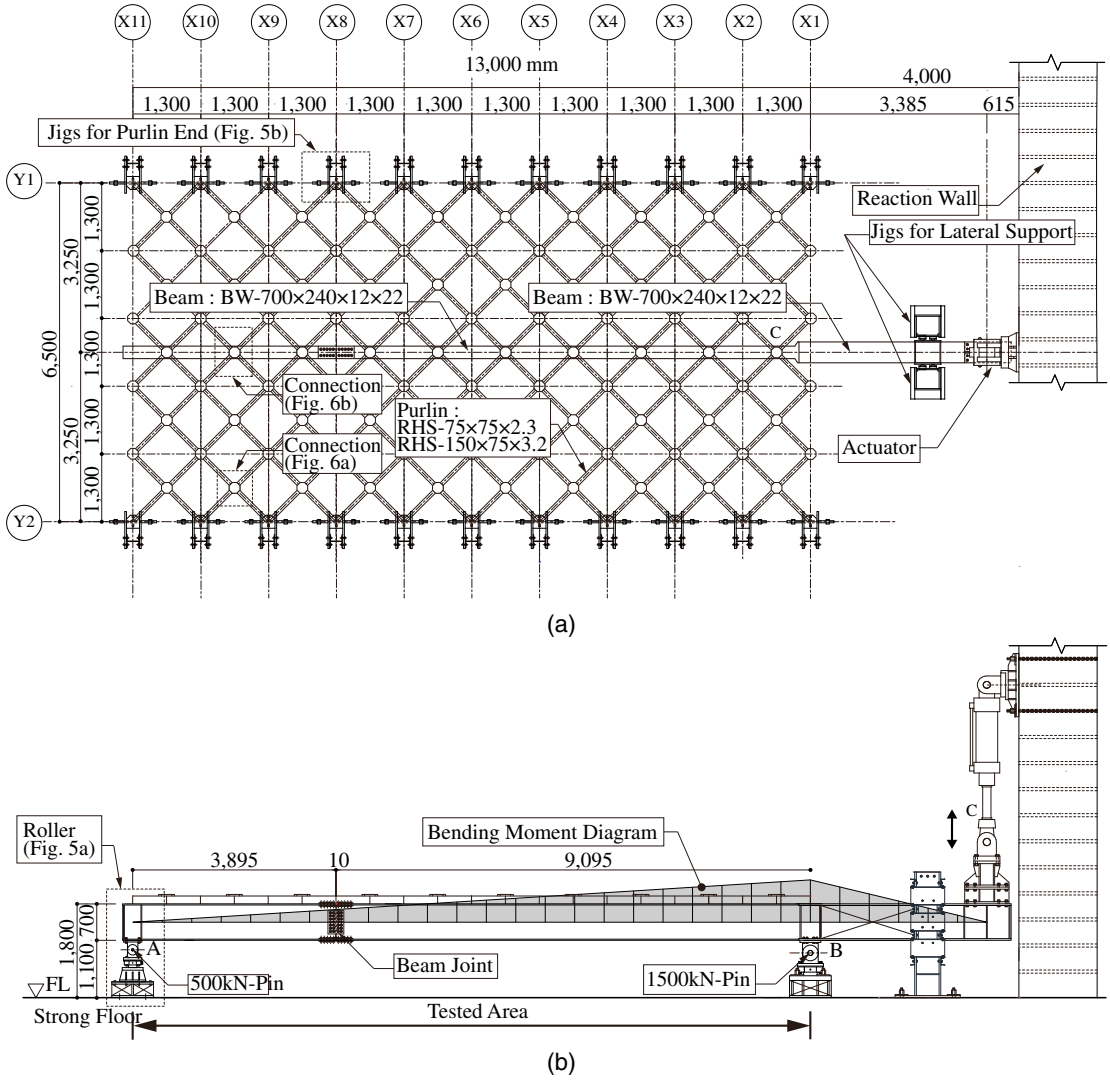

Fig. 3. Test setup: (a) plan view; and (b) elevation view.

[Point (b)]. In this study, this rotation was referred to as the *plastic rotation capacity*. Loss of strength followed after this plastic rotation capacity because of lateral-torsional buckling and local buckling [Point (c)] in the vicinity of the pin support B, as shown in Fig. 9(a). Although weld fracture occurred at the connection between the purlin at Point C (indicated in Fig. 3) to the top flange fractured at $\theta = 0.0664$ rad in the second cycle of $+3\theta_p$ [0.0664 rad, see Point (d)], the grid-purlin system showed ductile degrading hysteresis loops up to the second cycle of $\pm 5\theta_p$ (0.111 rad) after this weld was reinforced.

Fig. 4. Overall view of test setup. (Image by Toru Takeuchi.)

Fig. 8(b) shows that Specimen P75 also developed a maximum strength larger than the fully plastic moment [Point (a)]. The plastic rotation capacity was +0.048 rad in the positive part of the ninth cycle [Point (b)]. Local buckling was observed at an earlier stage in Specimen P75 than Specimen P150, and cracks in the purlin were observed at a rotation of 0.0475 rad [Point (c)]. However, the grid-purlin system demonstrated stable degrading hysteretic response up to the second cycle of $\pm 5\theta_p$ (0.111 rad).

Fig. 10 compares the lateral displacement of both specimens. The maximum lateral displacement of the top flange was not significant, suggesting the grid-purlin provided adequate stability bracing of the beams. Lateral-torsional buckling induced significant local deformation at the bottom flange. The maximum lateral displacement of Specimen P75 was larger than that of Specimen P150. In general, Specimen P150 exhibited better performance in ductility than P75. Nonetheless, both specimens have reached full plastic capacity and exhibited highly ductile behavior.

J. Struct. Eng., 2021, 147(7): 04021103

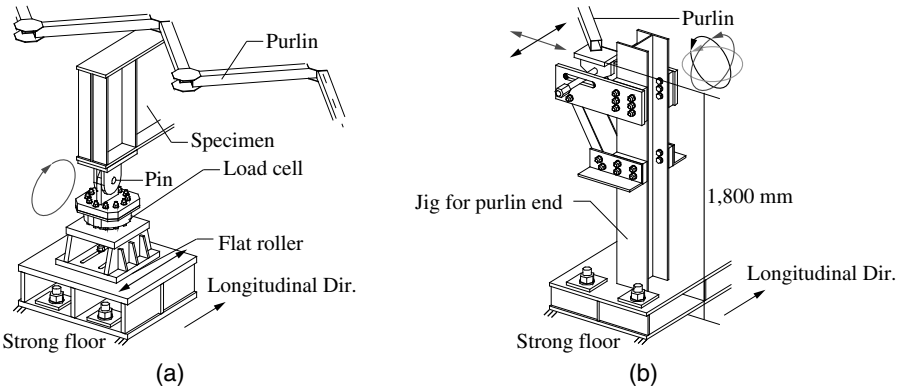

Fig. 5. Details of support jig for specimen: (a) pin and roller at 500-kN pin; and (b) jig for purlin end (Fig. 3).

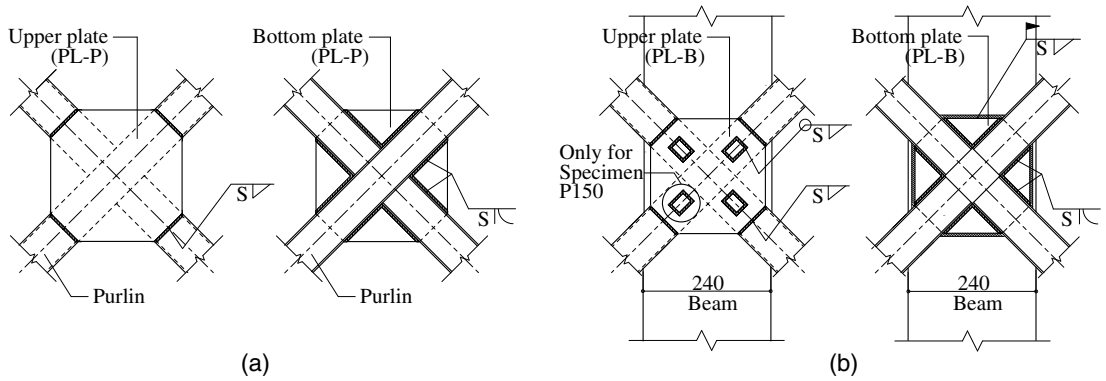

Fig. 6. Weld connections of purlin grid: (a) purlin-to-purlin weld connection; and (b) beam-to-purlin connection.

Table 1. Dimensions and material properties of RHS purlins

	Purlin					
	Section	Span		Material properties		
Label	RHS–$H \times B \times t$ (mm)	L (mm)	Steel grade	E (N/mm^2)	σ_y (N/mm^2)	σ_u (N/mm^2)
P150	RHS–150 × 75 × 3.2	1,300	STKR400	2.01×10^5	342	431
P75	RHS–75 × 75 × 2.3	1,300	STKR400	2.04×10^5	342	431

Note: H = depth; B = width; t = thickness; E = Young's modulus; σ_y = yield strength; and σ_u = ultimate strength.

Table 2. Dimensions and material properties of I-shaped beams

	I-shaped beam (W − $H \times B \times t_w \times t_f$)										
	Section				Flange					Max of L_b (mm)	
Label	BW–$H \times B \times t_w \times t_f$ (Built—W, mm)	L_a (m)	Steel grade	Part	E (N/mm^2)	σ_y (N/mm^2)	σ_u (N/mm^2)	r_y (mm)	M_p (kN·m)	MD	HD
P150	BW–700 × 240 × 12 × 22	13.0	SS400	Flange	1.96×10^5	280	449	5.2	1,438	668.3	334.2
				Web	1.97×10^5	301	464				
P75	BW–700 × 240 × 12 × 22	13.0	SS400	Flange	1.96×10^5	280	449	5.2	1,438	668.3	334.2
				Web	1.97×10^5	301	464				

Note: t_w = web thickness; t_f = flange thickness; L_a = length between pin and roller; MD = moderately ductile; HD = highly ductile; r_y = radius of gyration about weak axis; and M_p = fully plastic moment.

Table 3. Dimensions and steel grade of plates

Label	PL-P (plate) Section PL–$t \times B \times L_l$ (mm)	PL-P (plate) Steel grade	PL-B (plate) Section PL–$t \times B \times L_l$ (mm)	PL-B (plate) Steel grade	S (weld) Size (mm)
P150	PL–4.5 × 250 × 250	SS400	PL–3.2 × 205 × 205	SS400	4.5
P75	PL–4.5 × 220 × 220	SS400	PL–3.2 × 185 × 185	SS400	4.5

Note: L_l = Length.

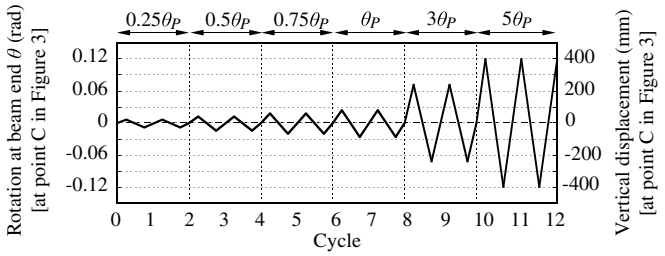

Fig. 7. Loading protocol for tests of grid-purlin specimens.

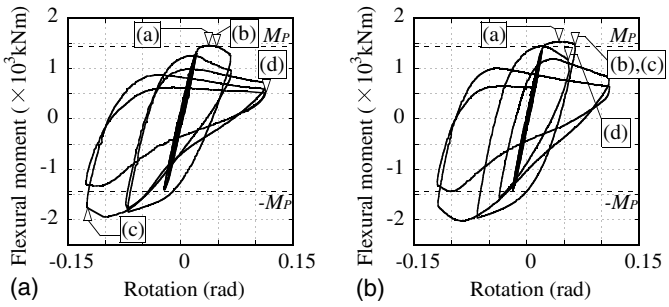

Fig. 8. Flexural moment-rotational angle relationship: (a) Specimen P150; and (b) Specimen P75.

Discussion on Plastic Rotation Capacity

In the commentary to D1.1 in ANSI/AISC 341-16 (AISC 2016a) states that highly ductile members are anticipated to experience plastic rotations of 0.04 rad or more. Therefore, the proposed grid-purlin system could be viewed as effective bracing for the stability of I-shaped beams. Both specimens could be rated as highly ductile even without the secondary beams' bracing.

Numerical Simulation for Reproducing Buckling Behavior of Test Specimens

Modeling

Fig. 11 illustrates the CFEM constructed on the Abaqus simulation platform. The beam and purlins were modeled with shell and beam elements, respectively. The purlins were connected rigidly to the top flange of the beam. Fig. 12 shows that the connection between the purlin and the top flange of the I-shaped beam included fillet welding and a steel plate. These were modeled using three directional springs. The stiffness in each direction was defined in Fig. 12. The strength in the z-direction was determined using Eq. (2) (AIJ 2012)

$$P_z = 1.4 \cdot \frac{t}{\sqrt{2}} \cdot \frac{F_u}{\sqrt{3}} \tag{2}$$

where t = thickness of steel plate at connection between purlin and top flange of I-shaped section; and F_u = ultimate strength of flange. For the I-shaped beam, the material nonlinearity was modeled using either a nonlinear kinematic hardening rule or a combined hardening rule with the Chaboche model shown in Eqs. (3)–(7)

$$\alpha_k' = C_k \frac{1}{\sigma^0}(\sigma - \alpha) \cdot |\varepsilon'^{pl}| - \gamma_k \alpha_k \cdot |\varepsilon'^{pl}| \tag{3}$$

$$\alpha = \sum_{k=1}^{N} \alpha_k \tag{4}$$

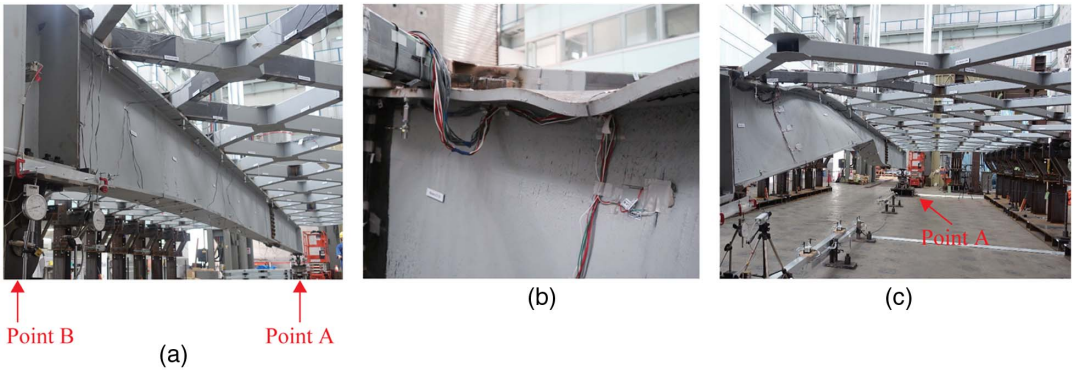

Fig. 9. Specimens during loading tests: (a) lateral buckling (Specimen P150, $+3\theta_p$); (b) local buckling (Specimen P150, $+5\theta_p$); and (c) lateral buckling (Specimen P75, $+5\theta_p$). [Reprinted with permission from Takeuchi et al. (2019).]

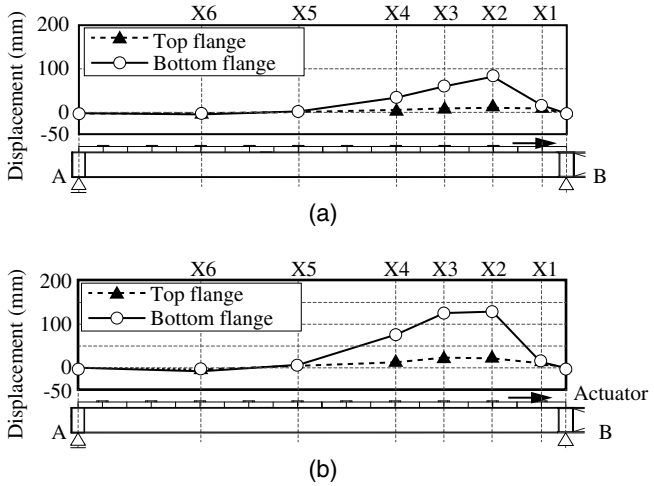

Fig. 10. Displacements of beams in out-of-plane direction: (a) purlin (P150: RHS 150 × 75 × 3.2); and (b) Purlin (P75: RHS 75 × 75 × 2.3).

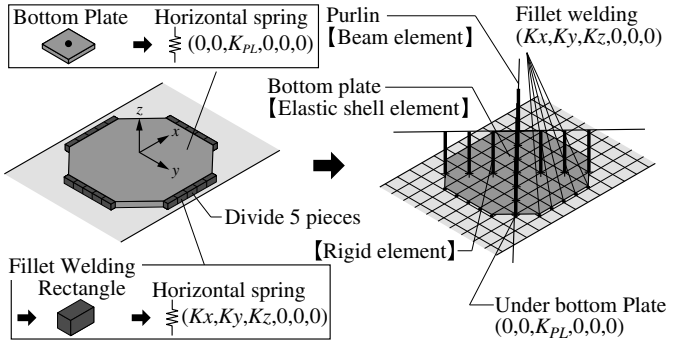

Fig. 12. Converting beam-to-purlin connection to CFEM.

$$\sigma^0 = \sigma|^0 + Q_\infty(1 - e^{-b|\varepsilon^{pl}|}) \tag{5}$$

where α_k' = backstress rate; C_k = initial kinematic hardening moduli; σ^0 = evolution of yield surface size; σ = stress; α = overall backstress; ε'^{pl} = equivalent plastic strain rate; γ_k = rate at which kinematic hardening modulus decreases with increasing plastic deformation; α_k = backstress of kinematic hardening component; $\sigma|^0$ = yield strength at zero plastic strain; Q_∞ = maximum change in size of yield surface; and b = rate at which size of yield surface changes as plastic strain develops. For the kinematic hardening rule, the maximum change in the size of the yield surface, Q_∞, was equal to zero. Table 4 lists the material parameters of the I-shaped beam for the aforementioned hardening rules. For the purlin, the material nonlinearity was modeled with isotropic hardening calibrated to the coupon test results. The elastic modulus and the Poisson's ratio of steel were 205,000 N/mm^2 and 0.3, respectively. The yield strength of the combined hardening material model was smaller than that of the material using the nonlinear kinematic hardening rule. Fig. 11(b) shows the initial imperfection of the I-shaped beam and the grid-purlin. The initial imperfection was introduced

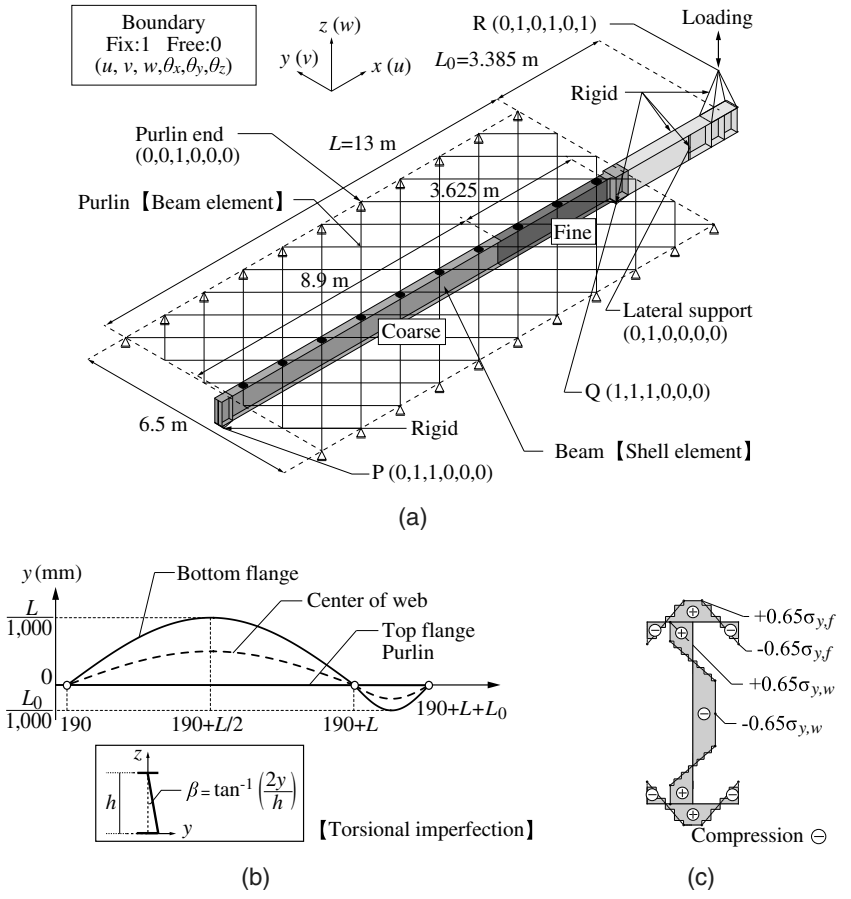

Fig. 11. FEM of grid purlin test specimen: (a) elements and boundary conditions; (b) initial imperfection; and (c) distribution of residual stress.

Table 4. Parameters for kinematic hardening in CFE analysis

Thickness (mm)	$\sigma\|_0$ (N/mm^2)	Kinematic hardening						Isotropic hardening	
		γ_1	C_1/γ_1 (N/mm^2)	γ_2	C_2/γ_2 (N/mm^2)	γ_3	C_3/γ_3 (N/mm^2)	Q_∞ (N/mm^2)	b
12, 16	170	250	37,500	10	1,600	1	307.5	80	5
22, 32	210								

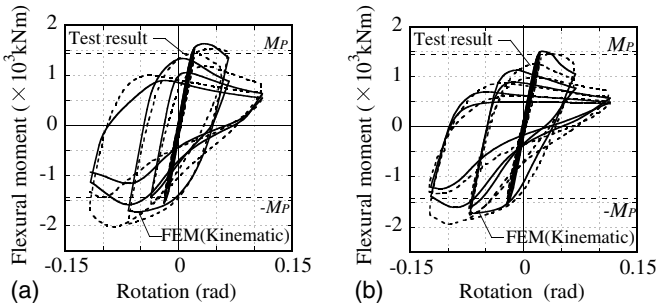

Fig. 13. Simulated versus experimental hysteresis (kinematic hardening): (a) P150; and (b) P75.

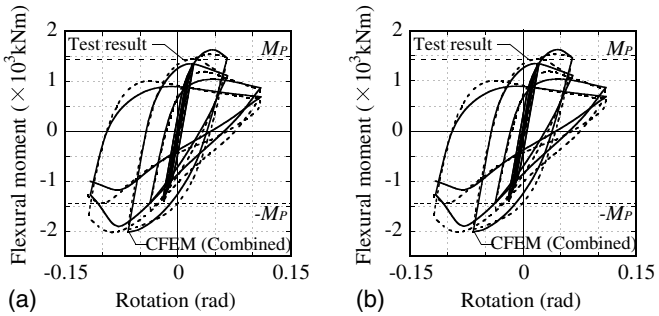

Fig. 14. Simulated versus experimental hysteresis (combined hardening): (a) P150; and (b) P75.

in order to initiate lateral-torsional buckling. The distribution of residual stress, as shown in Fig. 11(c), was used based on typical residual stress patterns (Ziemian 2010).

Simulated versus Experimental Results

Figs. 13 and 14 compare the simulated response versus the experimental hysteretic response. The simulated flexural moment versus rotation relation in Fig. 13 was calculated using nonlinear kinematic hardening. This did not accurately simulate the strength increment or stiffness reduction due to the Bauschinger effect after degradation. However, the simulated plastic rotation capacities for Specimens P150 and P75 were 0.068 and 0.04 rad, respectively, which were identical to the experimental results. Fig. 14 presents the simulated response using the combined hardening material model. The plastic rotation capacities for Specimens P150 and P75 were 0.075 and 0 rad, respectively, and did not accurately simulate the experimental results. Here, *0 rad* means that the flexural moments remained below the fully plastic moment strength. However, the combined hardening material model more precisely captured the hysteretic response after the strength degradation because it included the isotropic hardening.

Table 5. Dimension properties of CFE models for discussion of plastic rotation capacity

Beam section	Purlin section	Length
W − 390 × 300 × 10 × 16	No stiffening (N)	13.0 m
W − 488 × 300 × 11 × 18	RHS − 75 × 75 × 2.3 (P75)	15.6 m
W − 588 × 300 × 12 × 20	RHS − 125 × 75 × 2.3 (P125)	
W − 700 × 300 × 13 × 24	RHS − 150 × 75 × 2.3 (P150)	
W − 800 × 300 × 14 × 26		
W − 900 × 300 × 16 × 28		
W − 340 × 250 × 9 × 14		13.0 m
Built W − 700 × 240 × 12 × 22		

Plastic Rotation Capacity of I-Shaped Beams with Grid-Purlin

Profile for Parametric Study

Table 5 lists the parameters for the CFEMs of the steel I-shaped beams with grid-purlins to evaluate the plastic rotation capacity of the beams using the grid-purlins for lateral bracing. Sections of the I-shaped beam with a depth ranging from 390 to 900 mm and of purlins with a depth ranging from 75 to 150 mm were selected. These dimensions are typical of those used in construction. The model set consisted of eight types of beams and three types of purlin sections. The computational fluid dynamics (CFD) models in Fig. 15 were constructed using the element types, mesh densities, and initial imperfection shown in Figs. 11 and 12. The constitutive rules for the inelastic response were modeled based on the study of Ono and Sato (2000), as shown in Eqs. (6)–(9)

$$\sigma_n = E\varepsilon_n \quad (0 \le \varepsilon_n \le \varepsilon_{n,y}) \tag{6}$$

$$\sigma_n = \sigma_{n,y} \quad (\varepsilon_{n,y} \le \varepsilon_n \le \varepsilon_{n,st}) \tag{7}$$

$$\sigma_n = \frac{E}{\left(\frac{a}{\varepsilon_n}\right) + b} \quad (\varepsilon_{n,st} \le \varepsilon_n) \tag{8}$$

$$b = 3.79 + 0.945\left(\frac{E}{\sigma_u}\right) \tag{9}$$

where σ_n = engineering stress; $\sigma_{n,y}$ = nominal yield strength (258.5 N/mm^2); $\varepsilon_{n,y}$ = nominal yield strain; $\varepsilon_{n,st}$ = engineering strain at initiation of strain hardening; ε_n = engineering strain; a = material parameter (6.057); and b = material parameter. To evaluate the plastic rotation capacity of the beams with the grid-purlins, only nonlinear kinematic hardening rule was assigned for strain hardening based on the constitutive rule. The values of the material parameters were determined based on Japanese Industrial Standards SS400 and STKR400. The residual stress proposed by AIJ (2018) was introduced to the sections of the I-shaped beams. Unilateral and uniform loading were used for the CFEMs, as shown

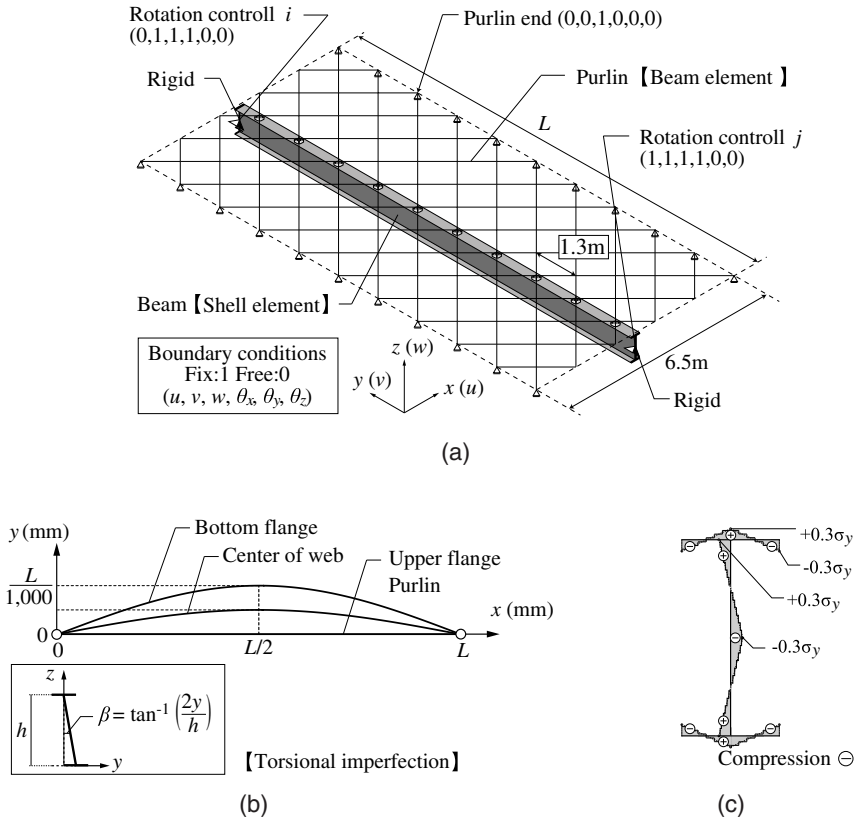

Fig. 15. FE component model with grid-purlin: (a) elements and boundary conditions; (b) initial imperfection; and (c) distribution of residual stress.

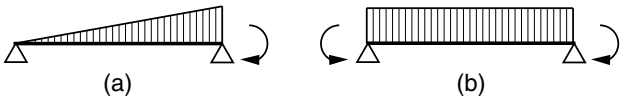

Fig. 16. Types of moment gradient: (a) unilateral loading; and (b) uniform loading.

in Fig. 16. Both moment gradients were single curvature bending. Pinned boundary conditions were used in the two directions.

Discussion on Plastic Rotation Capacity

Table 6 lists the plastic rotation capacities in each beam section combination with the grid-purlin system subjected to unilateral

Table 6. Plastic rotation capacity of I-shaped beams with grid-purlin

		Length: 13 m				Length: 15.6 m			
Loading pattern	Section	N	P75	P125	P150	N	P75	P125	P150
Unilateral loading	H340 × 250 × 9 × 14	0	0.148[a]	0.104[a]	0.103[a]	Plastic rotation capacity θ_{cp} (rad)			
	H390 × 300 × 10 × 16	0	0.113[a]	0.094[a]	0.093[a]	0	0.114[a]	0.096[a]	0.090 [a]
	H488 × 300 × 11 × 18	0	0.096[a]	0.111[a]	0.086[a]	0	0.096[a]	0.114[a]	0.089[a]
	H588 × 300 × 12 × 20	0	0.061[a]	0.074[a]	0.082[a]	0	0.059[a]	0.075[a]	0.085[a]
	H700 × 300 × 13 × 24	0	0.037[b]	0.047[a]	0.058[a]	0	0.035[b]	0.047[a]	0.059[a]
	H800 × 300 × 14 × 26	0	0.020[b]	0.033[b]	0.042[a]	0	0	0.032[b]	0.042[a]
	H900 × 300 × 16 × 28	0	0	0.021[b]	0.032[b]	0	0	0	0.033[b]
Uniform loading	H340 × 250 × 9 × 14	0	0.139[a]	0.112[a]	0.107[a]	Plastic rotation capacity θ_{cp} (rad)			
	H390 × 300 × 10 × 16	0	0.129[a]	0.111[a]	0.093[a]	0	0.142[a]	0.106[a]	0.098[a]
	H488 × 300 × 11 × 18	0	0.067[a]	0.103[a]	0.104[a]	0	0.074[a]	0.112[a]	0.098[a]
	H588 × 300 × 12 × 20	0	0	0.061[a]	0.082[a]	0	0	0.067[a]	0.087[a]
	H700 × 300 × 13 × 24	0	0	0	0.052[a]	0	0	0	0.056[a]
	H800 × 300 × 14 × 26	0	0	0	0.031[b]	0	0	0	0.037[b]
	H900 × 300 × 16 × 28	0	0	0	0	0	0	0	0

[a]Highly ductile.
[b]Moderately ductile.

loading and uniform loading with lengths of 13.0 and 15.6 m. These dimensions and properties are typical of those used in prior constructions. The I-shaped beams without a grid-purlin (N) exhibited no plastic rotation capacity because their strengths did not reach the plastic moment, M_p. The plastic rotation capacity of I-shaped beams with the grid-purlin increases as the depth of the I-shaped beams decreases and the height of the purlin increases. In this paper, plastic rotation capacities greater than 0.04 and 0.02 rad are referred to as highly ductile and moderately ductile, respectively, following seismic provisions in ANSI/AISC 341-16 (AISC 2016a). The plastic rotation capacity of many beams with the grid-purlins (P75, P125, P150) was greater than 0.04 or 0.02 rad, depending upon the purlin sizes, and met the requirements of highly ductile or moderately ductile members without using secondary beams. The number of beams capable of developing M_p with grid-purlins subjected to uniform loading was less than those subjected to unilateral loading.

Summary, Conclusions, and Limitations

This paper examines the plastic rotation capacity of I-shaped beams braced laterally by grid-purlins. Full-scale loading tests were performed to evaluate the strength and plastic rotation capacity of the beams with grid-purlins. CFE analysis was conducted to reproduce the response and investigate the performance of lateral bracing using grid-purlins for the I-shaped beams. The findings are summarized as follows:

1. In the test of the 13.0-m-long W-700 × 240 × 12 × 22 beam braced with a grid-purlin of RHS-150 × 75 × 3.2 with maximum spacing of L_b is 668 mm, corresponding to moderately ductile elements in the ANSI/AISC 341-16 (AISC 2016a), the beam experienced lateral-torsional and local buckling. With a grid-purlin, the bending strength of the beam reached a value larger than the fully plastic moment until the plastic rotation capacity reached approximately 0.065 rad without using secondary beam members. Even when the grid-purlin section was reduced to an RHS-75 × 75 × 3.2, the plastic rotation capacity reached approximately 0.045 rad. The grid-purlin of the specimens played a bracing role for the I-shaped beam. This satisfied the *highly ductile* rating defined in ANSI/AISC 341-16 (AISC 2016a).
2. For the CFEM using a kinematic hardening model for the constitutive rule of the yield surface, the simulated plastic rotation capacity was largely identical to the experimental plastic rotation capacity.
3. For I-shaped beam depths ranging from 340 to 900 mm and purlin widths ranging from 75 to 150 mm, the plastic rotation capacity of the I-shaped beams with the grid-purlin increased as the depth of the I-shaped beam decreased and the height of the purlin increased. Many combinations of the beams and the grid purlins typically used in construction satisfied the *highly ductile* and *moderately ductile* conditions defined in the AISC 341-16 provisions. The plastic rotation capacity under uniform loading was less than that under unilateral loading.

Both specimens of I-shaped beam with grid-purlin showed good strength and ductility performance. However, the boundary condition of the grid-purlins in the test setup was ideal for this performance. The grid-purlin system is commonly utilized as a nonstructural system for roof finishing to support cladding. It is not meaningful to compare the beam bracing performance of the grid-purlin system with that of the conventional system that have a few more secondary beams without grid-purlin systems. Although the fabrication work for the grid-purlin system requires sophisticated skill, the grid-purlin system has the benefit that it eliminates the construction process of secondary beams, which may lead to reductions in construction costs. This type of system has been used in a particular region in Japan. Based on the structural performance and cost-effectiveness of the system, it appears that this system shows potential for expanded use in the future, and the results can be extended to other types of roof purlins. The grid members in a grid-purlin should be parallel in general. However, when required by the structural load-path, grid members arranged in nonparallel configurations could be considered. The following two items reveal the beam bracing performance more deeply and alleviate the fabrication work of the grid-purlin system where future works are required: (1) physical tests or numerical simulations of grid-purlin systems with multiple spans; and (2) simplified fabrication skill for thin plate welding.

Data Availability Statement

Some data, computational models, or code generated or used during the study are available from the corresponding author by requests.

Acknowledgments

This research was supported by JST program on Open Innovation Platform with Enterprises, Research Institute of Academia. The authors thank Dr. Ching-Yi Tsai, a Post-doctoral fellow at National Taiwan Universtiy, and staffs in the National Center for Research on Earthquake Engineering, and Architecture and Building Research Institute, Ministry of the Interior in Taiwan, for their contributions to experiments conducted in this research. Any opinions, findings, and conclusions or recommendations expressed in this material are those of the authors and do not necessarily reflects the views of the sponsors.

References

AIJ (Architectural Institute of Japan). 2012. *AIJ recommendations for design of connections in steel structures*. Tokyo: AIJ.

AIJ (Architectural Institute of Japan). 2018. *AIJ recommendations for stability design of steel structures*. Tokyo: AIJ.

AISC. 2016a. *Seismic provisions for structural steel buildings*. ANSI/AISC 341-16. Chicago: AISC.

AISC. 2016b. *Specification for structural steel buildings*. ANSI/AISC 360-16. Chicago: AISC.

Bansal, J. P. 1971. "The lateral instability of continuous steel beams." CESRL dissertation, Dept. of Civil Engineering, Structures Research Laboratory, Univ. of Texas at Austin.

Kimura, Y., Y. Yoshino, and J. Ogawa. 2013. "Effect of lateral-rotational restraint and strength of continuously braces on lateral buckling load for H-shaped beams." [In Japanese.] *J. Struct. Constr. Eng.* 78 (683): 193–201. https://doi.org/10.3130/aijs.78.193.

Liu, D., M. Nakashima, and I. Kanao. 2003. "Behavior to complete failure of steel beams subjected to cyclic loading." *Eng. Struct.* 25 (5): 525–535. https://doi.org/10.1016/S0141-0296(02)00164-5.

Nakashima, M., I. Kanao, and D. Liu. 2002. "Lateral instability and lateral bracing of steel beams subjected to cyclic loading." *J. Struct. Eng.* 128 (10): 1308–1316. https://doi.org/10.1061/(ASCE)0733-9445(2002)128:10(1308).

Okazaki, T., D. Liu, M. Nakashima, and M. D. Engelhardt. 2006. "Stability requirements for beams in seismic steel moment frames." *J. Struct. Eng.* 132 (9): 1334–1342. https://doi.org/10.1061/(ASCE)0733-9445(2006)132:9(1334).

Ono, T., and A. Sato. 2000. "Modeling of stress-strain relationships of metallic materials." [In Japanese.] *J. Struct. Constr. Eng.* 65 (532): 177–184. https://doi.org/10.3130/aijs.65.177_2.

Takeuchi, T., R. Matsui, K. Koizmumi, P. C. Lin, M. Iwanaga, A. C. Wu, and K. C. Tsai. 2019. "Lateral buckling performance test of roof beam braced with grid-purlin system." In *Proc., 12th Pacific Structural Steel Conf.* Tokyo: Japanese Society of Steel Construction.

Yura, J. A. 2001. "Fundamental of beam bracing." *Eng. J.* 38 (1): 11–26.

Yura, J. A., T. V. Galambos, and K. Ravindra. 1978. "The bending resistance of steel beams." *J. Struct. Div.* 104 (9): 1355–1370. https://doi.org/10.1061/JSDEAG.0004982.

Ziemian, R. D. 2010. *Guide to stability design criteria for metal structures*. New York: Wiley.